Electronic Supplementary Material (ESI) for Chemical Communications

Low Temperature Phase Selective Synthesis of Cu_2ZnSnS_4 Quantum Dots

Christopher A. Cattley*, Cheng Cheng, Simon M. Fairclough, Laura M. Droessler, Neil P. Young, Jamie H. Warner, Jason M. Smith, Hazel Assender, Andrew A.R. Watt

Department of Materials, University of Oxford, Parks Road, Oxford, United Kingdom, OX1 3PH.

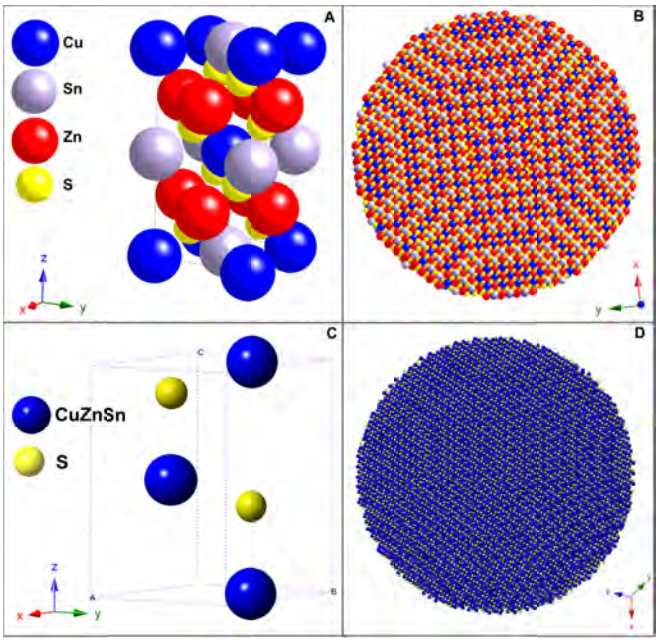

Figure S1 Unit cell of Cu_2ZnSnS_4 kesterite tetragonal a) and hexagonal (x2) b). 3D atomic model of a 10 nm Cu_2ZnSnS_4 nanoparticles with tetragonal c) and hexagonal d) structures.

Experimental

All chemicals were used without purification. Bis(trimethylsilyl) sulphide [TMSS] (Aldrich) and 1-octadecene [ODE] (Aldrich 99.5%) were stored in a nitrogen filled glovebox maintained at >10ppm O_2 and 0.1ppm H_2O atmospheric conditions. Due to the extremely volatile nature of TMSS, an appropriate quantity (0.475ml, 4mmol), for each reaction was diluted in 10ml of ODE and placed in sealed glass vials, inside the glovebox. The TMSS solution was then transferred to the reaction fume hood in an air tight, solvent resistant container immediately before it injected in to the reaction vessel, in order to limit oxidation and the risk of exposure to laboratory workers.

$Cu(C_5H_7O_2)_2$ (Aldrich 99.99%), $Zn(O_2CCH_3)_2$ (Aldrich 99.99%), $SnCl_4{\cdot}(H_2O)_5$ (Aldrich 98%) and oleylamine [OLA] (Aldrich 70%) were stored outside of a glovebox. In a typical preparation $Cu(C_5H_7O_2)_2$ (0.52mg, 2mmol), $Zn(O_2CCH_3)_2$ (29mg, 1mmol), $SnCl4{\bullet}(H_2O)_5$ (35mg, 1mmol) and OLA (20ml) are placed in a three neck flask and heated under vacuum and constant stirring to 75°C. The flask is then purged with argon as the temperature is increased to 130°C until a

yellowish transparent solution is formed, at which point these conditions are maintained for 1hr. After the reaction solution has reached the appropriate reaction temperature (140°C, 170°C or 190°C) the TMSS-ODE solution was injected in to the three neck flask. Immediately prior to injection the glass syringe is purged with argon 10 times to reduce the likelihood of oxygen/moisture entering the reaction vessel. Upon injection of the TMSS the reaction mixture changed from a yellow clear liquid to a thick brown colloid and the reaction solution temperature dropped 5-10°C. After 2 minutes of constant heat and continuous stirring the reaction vessel was removed from the heat and placed in an ice bath where it was allowed to cool below 60°C. A purged 10ml syringe was then used to transfer the nanoparticles colloid to a 50ml vial containing a 50/50 mix of hexane and methanol. The mixture was then agitated in an ultrasonic bath for 20mins and then allowed to separate before removing the un-reacted reagents suspended in the ethanol solution. This cleaning procedure was repeated several times before finally, the nanoparticles were dissolved in a variety of polar solvents to form thick, stable solutions. Aliquots were dispersed in hexane to form weak solutions (<1mg/ml) for characterization.

Characterisation

Transmission electron microscope samples were prepared by dipping an ultra-thin carbon coated gold grid into a very dilute solution of cleaned NCs dispersed in toluene/hexane. Each grid was oxygen plasma treated for 5 seconds, using a Nanotech PLASMOD plasma chamber, to remove any remaining organic material. Acquisition of low and high resolution images and selected area diffraction patterns was carried out using a JEOL-JEM 2010 LaB6 microscope, at an accelerating voltage of 200 kV. Scanning transmission electron microscopy elemental mapping and high angle annular dark field imaging was carried out using a JEOL 3000F field emission gun microscope at an accelerating voltage of 300kV (equipped with an Oxford Instruments LZ5 windowless energy dispersive X-ray spectrometer). Imaging of individual lattice planes and corresponding twinning analysis of CZTS nanoparticles was carried out using a Oxford-JEOL 2200MCO aberration corrected microscope. XRD analysis was performed using a Philips Theta-2-Theta X-ray diffractometer. Samples were prepared by drop casting thick (>100mg/ml) NC dispersions onto 25x25mm silicon

wafers. UV-Vis photo-absorption measurements were performed using a Varian Cary 5000i UV-VIS-NIR spectrometer. Samples were prepared by dissolving CZTS nanoparticles in hexane/toluene to form weak solutions (1mg/ml), which were then spin-cast onto quartz slides which were then oxygen plasma treated for 30seconds for spectral analysis.DTA/TGA analysis was carried out using a Perkin Elmer Pyris1 TGA. Samples were prepared by pipetting 30mg/ml solutions, of CZTS nanocrystals in hexane, in to 50ηl ceramic crucible. Raman spectroscopy analysis was carried out using a JY Horiba LabRAM ARAMIS imaging confocal Raman microscope. Samples were prepared by drop casting 30mg/ml solutions of CZTS nanocrystals in hexane on to silicon wafer substrates and allowing for the hexane to evaporate, thus forming a thin CZTS nanocrystal film.

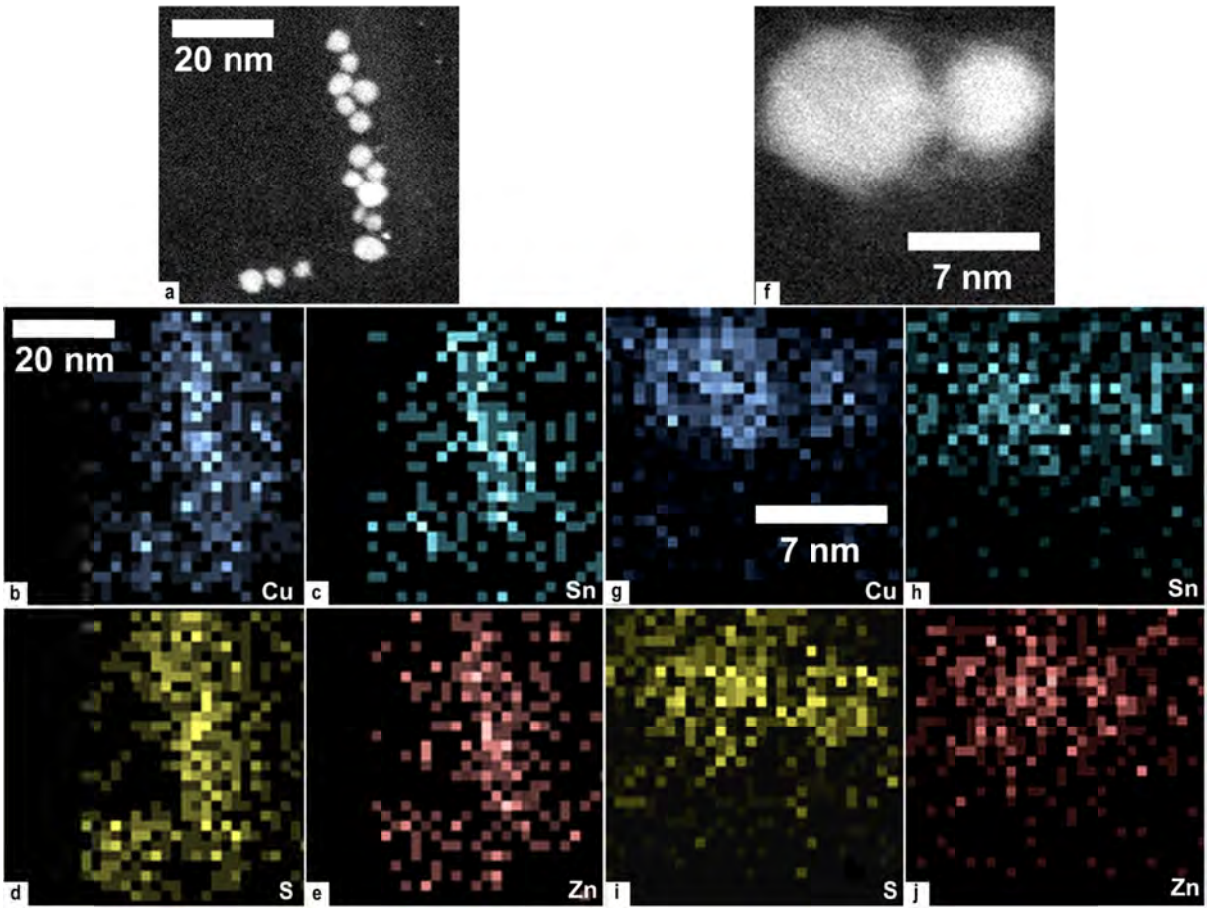

Figure S2: a,f) High angle annular dark field (HAADF) STEM image of CZTS nanoparticles nucleated at 170°C/190°C respectively. b-e, g-j) STEM-EDX elemental mapping micrographs identifying Sn, Cu, Zn and S present in each respective nanoparticles sample.

EDX elemental mapping was carried out using a 1nm probe diameter. To estimate the relative elemental composition of each nanoparticle sample, multiple line profiles were taken across each

elemental STEM-EDX map; the average X-ray yields were estimated from the greyscale count from each micrograph and multiplied by the Z number to obtain an effective composition ratio. The results of this analysis are displayed in Table 1 below.

Table 1: Analysis of average X-Ray yield from STEM EDX elemental micrographs

Element	Gray Scale Count (0-256) - X-ray yield			Ratio		
Cu	250.19	106.02	118.84	2.00	2.00	2.00
Zn	139.18	57.59	67.03	1.08	1.05	1.09
Sn	203.72	88.04	99.57	0.94	0.96	0.97
S	246.77	104.53	123.37	3.58	3.57	3.76
Temp.	140°C	170°C	190°C	140°C	170°C	190°C

The data summarised in Table 1 suggests that the composition of each nanoparticles sample is approximately stoichiometric Cu_2ZnSnS_4. Each sample also shows significant S deficiency compared with the purely stoichiometric Cu_2ZnSnS_4 ratio.

Due to the poor signal to noise ratio, apparent in the XRD spectra, we were unable to accurately utilise the Scherrer equation to estimate the average grain size, and therefore confirm the average nanoparticle diameter of each sample as estimated using TEM micrograph analysis. The absence of the strongly diffracting 002 and 102 peaks from the spectra taken at 170°C and 190°C may suggest that these nanocrystals not-isotropic despite how they appear what was observed during TEM characterisation.

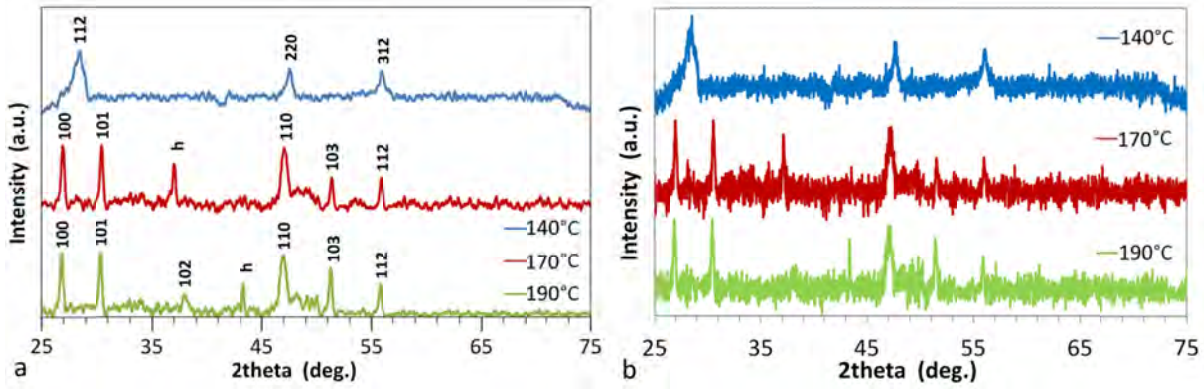

Figure S3: X-Ray diffraction traces of CZTS QDs synthesized at 140°C, 170°C and 190°C a) with and b) without background correction.

Background removal was applied to the raw XRD spectra using Xpert-Highscore spectroscopy analysis software. The raw spectra are shown in Figure S3 below and the

crystallographic parameters of the model used to analyse the Hexagonal CZTS structure, calculated using Crystalmaker Software from the lattice parameters published by Lu et al[1], are shown in Table 2.

Table 2: Calculated crystallographic parameters for the Hexagonal CZTS structure

Wurtzite			d [A]	2 θ	Intensity
0	1	0	3.32441	26.7938	77.61
0	0	2	3.1694	28.1305	51.03
0	1	1	2.94409	30.3331	85.64
0	1	2	2.29395	39.2393	30.46
1	1	0	1.91935	47.3199	60.49
0	1	3	1.78323	51.1815	62.23
0	2	0	1.66221	55.2122	9.29
1	1	2	1.64177	55.9594	41.01
0	2	1	1.60784	57.2477	13.82
0	0	4	1.5847	58.1631	1.61
0	2	2	1.47204	63.1013	6.96
0	1	4	1.43049	65.1567	1.65
0	2	3	1.30641	72.2563	20.84
1	2	0	1.25651	75.6146	6.94
1	2	1	1.23253	77.3549	10.46
1	1	4	1.22201	78.1467	3.57
0	1	5	1.18455	81.1205	14.97

DTA-TGA analysis was carried out to help determine whether the synthesised nanocrystals were pure CZTS or a combination of CTS and ZnS nanocrystals. The data presented in Figure S3a suggests there is a single transition for each sample at approximately ~ 830°C. For each sample, the presence of additional transitions at lower temperatures (<500°C) may suggest the presence of unreached precursors, left over from the each synthesis, which undergo oxidation at these temperatures.

The results of Raman scattering analysis shown in Figure S3b suggest that a single crystalline species of CZTS is present in each sample. All three spectra display an intense peak in the 331-338cm^{-1} region associated with bulk CZTS. The intense peak observed for the sample nucleated at 140°C (tetragonal CZTS) had a fractionally higher peak position compared to those samples nucleated at 170°C and 190°C (hexagonal CZTS). The different Raman shift values for tetragonal and hexagonal CZTS would suggest that the characteristic peak for hexagonal CZTS may differ from that

of tetragonal[2]. This phenomenon may be caused by the different arrangements of atoms in each respective crystal structure. Apart from the above mentioned Raman peaks, no other characteristic peaks of impurities were observed such as $Cu_{1.97}S$ (475 cm^{-1}) ZnS (351 and 274cm^{-1}) Cu_3SnS_4 (318,348 and 295cm^{-1}), SnS_2 (315 cm^{-1})[3–6].

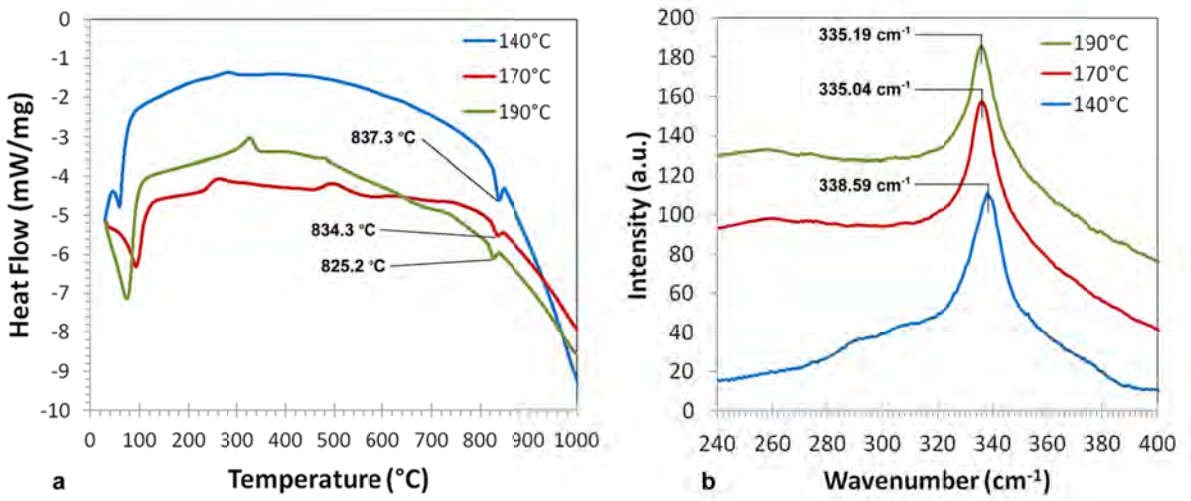

Figure S4: a) DTA/TGA analysis and b) Raman spectra of CZTS nanocrystals nucleated at 140°C, 170°C and 190°C.

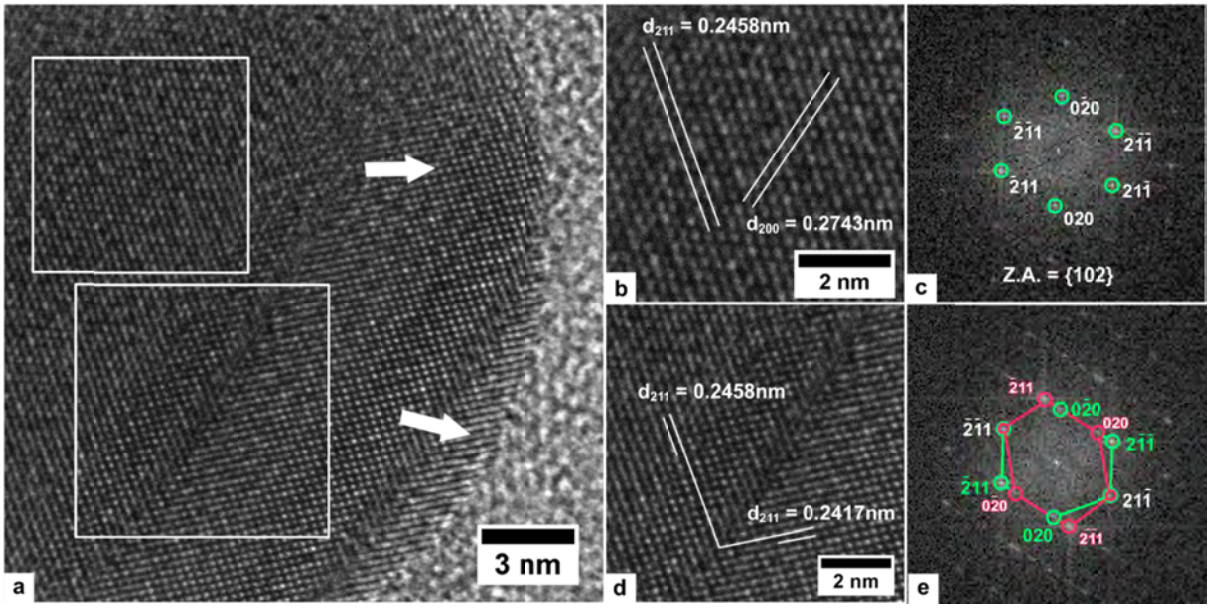

Figure S5: a) HRTEM images of CZTS nanocrystals nucleated at 140°C, b) enlarged micrograph and c) corresponding Fourier transform of an un-twinned region with indexed interplanar spacings of 0.2458nm and 0.2743nm, which correspond to the (211) and (200) planes respectively, d) enlarged micrograph of a twinned region and e) corresponding Fourier transform with indexed interplanar spacing of 0.2417nm and 0.2458nm which correspond to the twinned (211) planes of the tetragonal CZTS structure.

The presence of a twin formation in the tetragonal structure of an aged CZTS nanocrystal has been identified using HRTEM (Figure S5). The intersecting planes of the untwined region have been indexed to be (211) and (200) respectively. By comparing the Fourier transforms of both the twinned and untwined regions of the crystal, the twin transformation about the 102 zone axis has been indexed. The identification of twinning within the crystal structure would suggest that significant strain has built up during the growth of the nanocrystal, which is relieved by the presence of twins in the crystal structure.

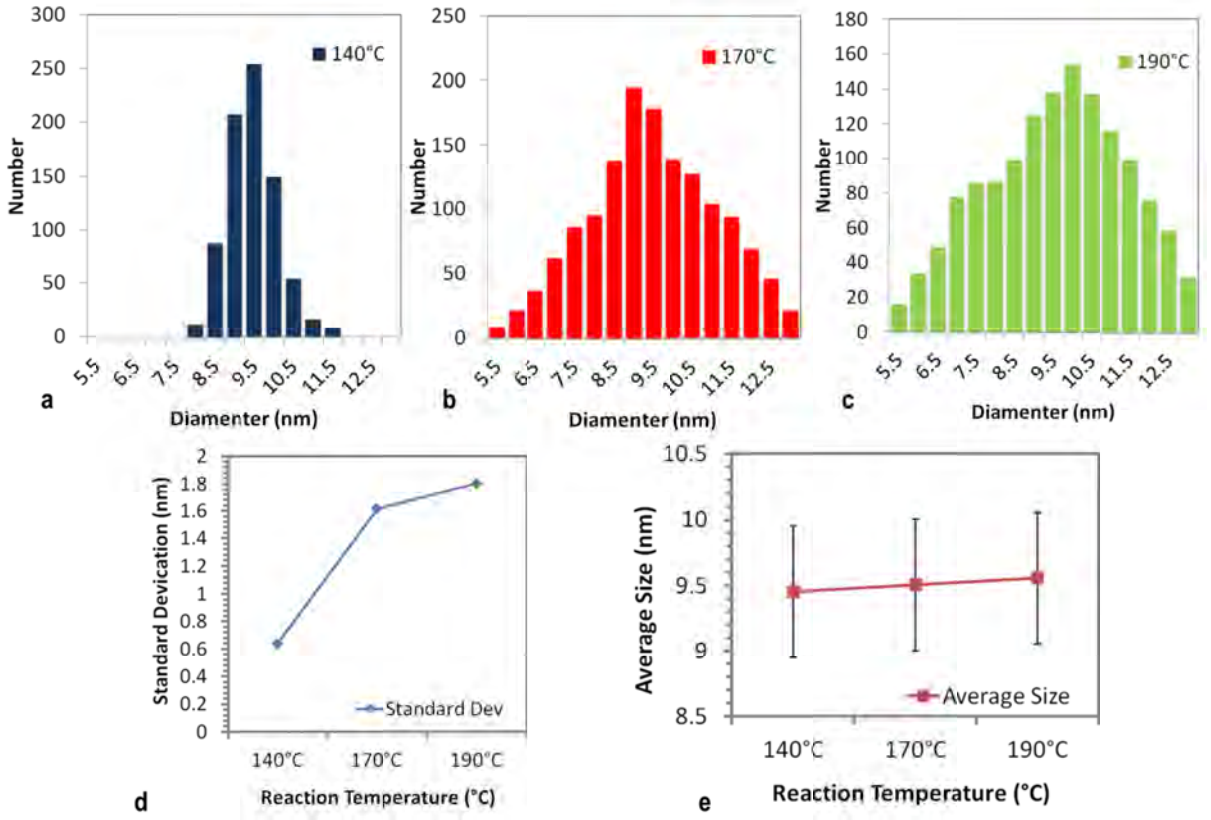

Figure S6: a-c) Size distribution analysis of low resolution TEM micrographs of CZTS samples nucleated at 140°C, 170°C and 190°C. d-e) Graphs of standard deviation and average (mean) nanoparticle diameter with increasing nucleation temperature. The error bars in e) represent the categorisation of nanoparticles into 0.5nm size groups for counting.

Existing experimental data devoted to the characterisation of the optical properties of CZTS provide inconsistent values for the band gap of this material system. The majority of the experimentally determined values are between 1.4 and 1.5 eV. An extended discussion on the band gap values of CZTSe and CZTS is reported elsewhere[7]. Previous studies have theoretically calculated the band gaps of CZTS and CZTSe, and concluded that the band gap of CZTS should be around 1.5

eV[8], which is consistent with the experimental value for CZTS nanoparticles prepared using this method. Further investigation of how the composition affects the band gap of these CZTS nanoparticles is needed. The band gap of kesterite is calculated to be larger than that of stannite CZTS whereas the hexagonal (wurtzite) derived kesterite structure is predicted to be larger than the tetragonal structure[9]. However, these values have yet to be confirmed by experimental measurement to a high degree of accuracy, indeed a number of researchers report that the crystal structure has a negligible effect on the band gap[10]. However, through our synthesis route we provide evidence to suggest that the phase of the CZTS nanoparticles does affect the band gap of the material.

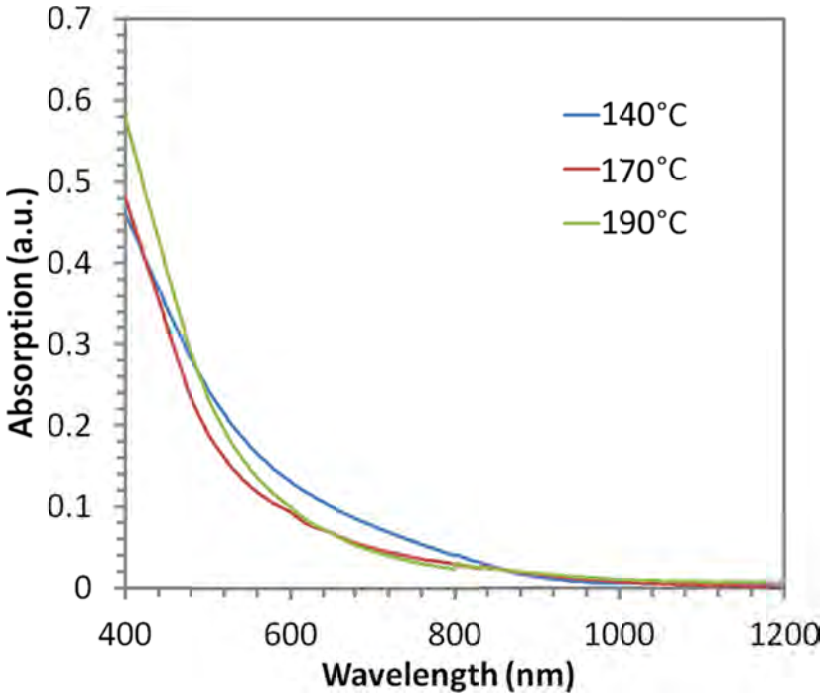

Figure S7: UV-VIS absorbance spectrum of the CZTS nanoparticles synthesised at 140°C, 170°C and 190°C.

References

(1) Lu, X.; Zhuang, Z.; Peng, Q.; Li, Y. *Chemical Communications* **2011**, *47*, 3141–3.

(2) Li, M.; Zhou, W.-H.; Guo, J.; Zhou, Y.-L.; Hou, Z.-L.; Jiao, J.; Zhou, Z.-J.; Du, Z.-L.; Wu, S.-X. *The Journal of Physical Chemistry C* **2012**, *116*, 26507–26516.

(3) Katagiri, H.; Jimbo, K.; Maw, W. S.; Oishi, K.; Yamazaki, M.; Araki, H.; Takeuchi, A. *Thin Solid Films* **2009**, *517*, 2455–2460.

(4) Regulacio, M. D.; Ye, C.; Lim, S. H.; Bosman, M.; Ye, E.; Chen, S.; Xu, Q.-H.; Han, M.-Y. *Chemistry (Weinheim an der Bergstrasse, Germany)* **2012**, *18*, 3127–31.

(5) Jiang, H.; Dai, P.; Feng, Z.; Fan, W.; Zhan, J. *Journal of Materials Chemistry* **2012**, *22*, 7502.

(6) Grossberg, M.; Krustok, J.; Raudoja, J.; Timmo, K.; Altosaar, M.; Raadik, T. *Thin Solid Films* **2011**, *519*, 7403–7406.

(7) Walsh, A.; Chen, S.; Gong, X. G.; Wei, S. *Solar Cells 4*, 4–5.

(8) Chen, S.; Walsh, A.; Yang, J.-H.; Gong, X.; Sun, L.; Yang, P.-X.; Chu, J.-H.; Wei, S.-H. *Physical Review B* **2011**, *83*, 1–5.

(9) Chen, S.; Walsh, A.; Luo, Y.; Yang, J.-H.; Gong, X.; Wei, S.-H. *Physical Review B* **2010**, *82*, 1–8.

(10) Repins, I.; Vora, N.; Beall, C.; Wei, S.; Yan, Y.; Romero, M.; Teeter, G.; Du, H.; To, B.; Young, M. *Renewable Energy* **2011**.